INTERNATIONAL JOURNAL OF REMOTE SENSING, 2017
VOL. 38, NO. 23, 7281–7301
https://doi.org/10.1080/01431161.2017.1372860

Taylor & Francis
Taylor & Francis Group

A WTLS-based rational function model for orthorectification of remote-sensing imagery

Yong Ge[a], Yongzhao Wei[b], Yongze Song[c], Tianjun Wu[b], Alfred Stein[d], Xian Guo[a], Chenghu Zhou[a] and Jianghong Ma[b]

[a]State Key Laboratory of Resources and Environmental Information System, Institute of Geographical Sciences and Natural Resources Research, Chinese Academy of Sciences, Beijing, China; [b]Department of Mathematics and Information Science, Chang'an University, Xi'an, China; [c]Australasian Joint Research Centre for Building Information Modelling, School of Built Environment, Curtin University, Perth, Australia; [d]Faculty of Geo-Information Science and Earth Observation (ITC), University of Twente, Enschede, Netherlands

ABSTRACT

The rational function model (RFM) is widely applied to orthorectification of aerial and satellite imagery. This article proposes a new method named Ortho-WTLS to solve the RFM in remote-sensing imagery orthorectification. Based on a weighted total least squares (WTLS) estimator, the proposed method allows one to handle coordinates of ground control points (GCPs) that contain errors and are of unequal accuracies. This situation occurs, e.g. if GCPs are automatically selected. In the proposed model, first, the relationship of two linearization methods for an RFM with errors contained in GCPs is investigated and results in a hybrid linearization. Next, based on WTLS, RFM coefficients are estimated with an iterative computation function. Finally, the performance of the Ortho-WTLS method thus obtained is investigated using simulated images and remotely sensed images by collecting GCPs with varying errors. Experimental results show that the Ortho-WTLS method achieves a more robust estimation of model parameters and a higher orthorectification accuracy when compared with standard LS-based RFM estimation. We conclude that the quality of GCPs has a large impact on the accuracy and that an increasing number of low-precision GCPs may lead to a decrease in orthorectification quality.

ARTICLE HISTORY
Received 26 December 2016
Accepted 21 August 2017

1. Introduction

Remote sensing presents an important way to access geo-spatial information. Remote-sensing images, however, become aberrant and distorted during capturing due to factors such as the Earth's rotation, sensor attitude, and terrain conditions (Toutin 2003; Ge et al. 2006). These aberrations and distortions have a significant impact on both quality of images and subsequent analysis and decision-making (Li et al. 2016). Therefore, it is necessary to perform rectification on the images to reduce or eliminate the aberrations and distortion prior to further processing (Richards and Jia 1999). The methods of geometric correction, image

CONTACT Yong Ge gey@lreis.ac.cn; Xian Guo guoxian@lreis.ac.cn State Key Laboratory of Resources and Environmental Information System, Institute of Geographical Sciences and Natural Resources Research, Chinese Academy of Sciences, China

registration, and orthorectification have been developed recently for different applications with various terrain conditions (Toutin 2004; Dave, Joshi, and Srivastava 2015). Geometric correction and image registration can effectively correct geometric distortions, when applied to images acquired from relatively flat terrain. For study areas with undulating terrains, where image distortion caused by terrain properties is more difficult to eliminate, orthorectification methods are developed to address these terrain-caused distortions (Tao and Hu 2001a).

The common process in both geometric correction models and orthorectification models is collecting corresponding ground control points (GCPs) in a study area. GCPs are mainly collected from GIS data and remote-sensing images and essentially contain errors due to the errors in data acquisition. Such errors will then propagate towards the corrected image during geometric correction and orthorectification and lead to biased coefficient estimation (Ge et al. 2006; Tong, Jin, and Li 2011; Ge et al. 2012; Wu et al. 2015). Recently, a series of studies on addressing errors in coefficients for geometric correction has been conducted. Methods based on consistent adjusted least squares estimation, relaxed consistent adjusted least squares estimation (Ge et al. 2006), total least squares (TLS) (Ge et al. 2006; Wansbeek and Meijer 2000; Van Huffel and Vandewalle 1991; Matei and Meer 2006), and scale TLS (STLS) were designed. The above methods are based on the errors-in-variables (EIV) model and address independent variables that contain errors (Ge et al. 2012). Among them, STLS estimation is effective in determining the relative error sizes of response and explanatory variables by including a scaling factor (Paige and Strakoš 2002). However, the precision of GCPs may vary in image registration, when some GCPs are simultaneously obtained from both fine scale and coarse-scale maps (Wu et al. 2015), resulting in measurement errors having a non-identical distribution. This situation cannot be effectively addressed by STLS estimation (Likar and Pernuš 1999; Abdelsayed, Ionescu, and Goodenough 1995). To solve this problem, weighted total least squares (WTLS) estimation was proposed to address heteroscedastic data structures in the EIV model (Markovsky et al. 2006), and iteration weight TLS estimation as a more effective and robust method for geometric correction (Wu et al. 2015) was further investigated.

Orthorectification models for remote-sensing images primarily include collinear equation models, 3D polynomial models, and rational function models (RFMs). RFMs are commonly used as non-linear models and widely applied for processing various types of sensors (Toutin 2004). RFMs need to be linearized before performing remote-sensing image orthorectification (Tao and Hu 2001a; Dowman and Dolloff 2000). At present, two primary RFM linearization methods are commonly used (Dowman and Dolloff 2000), but their relationships and applicability have not been discussed before. Moreover, LS estimation is commonly adopted in RFMs linearization. When GCPs contain errors, LS estimator is no longer applicable to solve the biased estimation of model coefficients, which should be addressed by EIV model. In addition, little research has been carried out on the impact of GCPs with errors exhibiting a heteroscedastic structure on the orthorectification for remote-sensing images.

To overcome the above problems, this article introduces the Ortho-WTLS method for RFMs to perform remote-sensing image orthorectification. It addresses the heteroscedastic error structure of GCPs and handles biased estimation in orthorectification. In this article, two RFM linearization methods, together with their relationships, are first introduced and a hybrid linearized RFM is comparatively derived. The proposed Ortho-WTLS

method estimates the RFM coefficients based on WTLS and the structure of the hybrid RFM; thus, the errors of the observation and the errors of the coefficients are both taken into consideration. Furthermore, the effectiveness of the Ortho-WTLS is validated with simulated and real remote-sensing images. Finally, the impacts of the quantity and the quality of GCPs on the precision of orthorectification are analysed.

2. Ortho-WTLS method for image orthorectification

2.1. *RFM theory*

The RFM provides image coordinates (U_x, U_y) as the ratios of polynomials, with the independent variables related to the corresponding ground coordinates (G_x, G_y, G_z). The highest order is usually taken to be equal to three. The model equation is (Consortium 1999; 2004; Yang 2000; Tao and Hu 2001b)

$$\begin{cases} U_x = \dfrac{P_1(G_x,G_y,G_z)}{P_2(G_x,G_y,G_z)} = \dfrac{\boldsymbol{Ha}^{\mathrm{T}}}{\boldsymbol{Hb}^{\mathrm{T}}} \\ U_y = \dfrac{P_3(G_x,G_y,G_z)}{P_4(G_x,G_y,G_z)} = \dfrac{\boldsymbol{Hc}^{\mathrm{T}}}{\boldsymbol{Hd}^{\mathrm{T}}} \end{cases} \tag{1}$$

where ***a, b, c***, and ***d*** are rational polynomial coefficients (RPCs), i.e. coefficient vectors of the RFM, and ***H*** is the vector composed of ground coordinates. Third-order polynomial is most commonly used in an RFM.

Equation (1) expresses the relationship between the true value of the pixel coordinate (U_x, U_y) and that of (G_x, G_y, G_z). Due to measurement errors associated with the image coordinate $\varepsilon = (\varepsilon_x, \varepsilon_y)$ and those with the ground coordinate $\delta = (\delta_x, \delta_y, \delta_z)$, only the corresponding observations are available, recorded as $u = (u_x, u_y)$ and $\boldsymbol{m}$ is the vector composed of ground coordinates (g_x, g_y, g_z). Therefore, the measurement errors corresponding to the RFM are therefore expressed as

$$\begin{cases} \varepsilon_x = \hat{u}_x - u_x = \dfrac{P_1(g_x,g_y,g_z)}{P_2(g_x,g_y,g_z)} - u_x = \dfrac{\boldsymbol{ma}^{\mathrm{T}}}{\boldsymbol{mb}^{\mathrm{T}}} - u_x \\ \varepsilon_y = \hat{u}_y - u_y = \dfrac{P_3(g_x,g_y,g_z)}{P_4(g_x,g_y,g_z)} - u_y = \dfrac{\boldsymbol{mc}^{\mathrm{T}}}{\boldsymbol{md}^{\mathrm{T}}} - u_y \end{cases} \tag{2}$$

The RFM is clearly a non-linear equation with unknown coefficients, and LS together with its generalizations (WLS, TLS, or WTLS) are effective tools for its linear iteration.

2.2. *A hybrid RFM linearization*

Two RFM linearization methods, together with their relationships, will be introduced in this section. The first method is an iteration of initial values. Initial values are set, and then the linearized RFM is calculated iteratively (Tao and Hu 2001a; Gong and Zhang 2003). The error equation of u_x derived from (2) equals

$$\varepsilon_x = \hat{u}_x - u_x = \frac{\boldsymbol{ma}^{\mathrm{T}}}{\boldsymbol{mb}^{\mathrm{T}}} - u_x \tag{3}$$

Linearizing (3) with the initial value iteration method results in Equation (4).

$$\varepsilon_x = \frac{\boldsymbol{m}\boldsymbol{a}^{\mathrm{T}}}{\boldsymbol{m}\boldsymbol{b}^{\mathrm{T}}} - \frac{u_x}{\boldsymbol{m}\boldsymbol{b}^{\mathrm{T}}}\boldsymbol{m}\boldsymbol{b}^{\mathrm{T}} = \frac{[\boldsymbol{m}, \quad -\boldsymbol{u_x}\boldsymbol{m}]\left[\boldsymbol{a}^{\mathrm{T}}, \quad \boldsymbol{b'}^{\mathrm{T}}\right]^{\mathrm{T}}}{\boldsymbol{m}\boldsymbol{b}^{\mathrm{T}}} - \frac{\boldsymbol{u_x}}{\boldsymbol{m}\boldsymbol{b}^{\mathrm{T}}} \tag{4}$$

where b' is a vector defined by the relationship: $\boldsymbol{m}\boldsymbol{b'}^{\mathrm{T}} + \boldsymbol{1} = \boldsymbol{m}\boldsymbol{b}^{\mathrm{T}}$. Setting $D = \boldsymbol{m}\boldsymbol{b}^{\mathrm{T}}$, $\boldsymbol{\beta_x} = \left[\boldsymbol{a}^{\mathrm{T}}, \quad \boldsymbol{b'}^{\mathrm{T}}\right]^{\mathrm{T}}$, and $\boldsymbol{v} = [m, \quad -u_x\boldsymbol{m}]$, we obtain

$$\varepsilon_x = \frac{\boldsymbol{v}}{D}\boldsymbol{\beta_x} - \frac{u_x}{D} \tag{5}$$

Equation (5) is the RFM error equation including pixel coordinates and plane coordinates. The matrix form of the error equation is given by Equation (6) where sample data of n GCPs are substituted into Equation (5),

$$\boldsymbol{\varepsilon}_x = \mathbf{D}^{-1}\mathbf{v}\boldsymbol{\beta}_x - \mathbf{D}^{-1}\boldsymbol{u}_x \tag{6}$$

where $\varepsilon_x = [\varepsilon_{x_1}, \varepsilon_{x_2}, \ldots, \varepsilon_{x_n}]^{\mathrm{T}}$, $\mathbf{v} = [\boldsymbol{v}_1, \boldsymbol{v}_2, \ldots, \boldsymbol{v}_n]^{\mathrm{T}}$, $\boldsymbol{u}_x = [u_{x_1}, u_{x_2}, \ldots, u_{x_n}]^{\mathrm{T}}$, and $\mathbf{D}^{-1} = \mathrm{diag}\left(\left[D_1^{-1}, D_2^{-1}, \ldots, D_n^{-1}\right]\right)$. To iteratively process Equation (6), the initial value $\mathbf{D}^{-1(0)}$ of $\mathbf{D}^{-1}$ is set as a unit matrix, resulting in a linear equation. LS is used to derive the initial value of the RPC $\boldsymbol{\beta}_x^{(0)}$, where $\boldsymbol{\beta}_x^{(0)} = \left[\left(a^{(0)}\right)^{\mathrm{T}} \quad \left(b'^{(0)}\right)^{\mathrm{T}}\right]^{\mathrm{T}}$. Next, $\mathbf{D}^{-1(1)} = \mathrm{diag}\left(1/\boldsymbol{v_i}\boldsymbol{b}^{(0)\mathrm{T}}\right)$ is obtained, and $\boldsymbol{\beta}_x{}^{(1)}$ is derived from LS estimation. Iteration is repeated until all correcting numbers are smaller than a given threshold. This iteration process for RFM linearization, however, is complex because it requires both initial values and performing the iterative calculations.

Another linearization method can be found in Qin et al. (2005) and Dowman and Dolloff (2000). This method transforms Equation (1) as

$$F_{\boldsymbol{u}_x} = P_1\left(G_x, G_y, G_z\right) - \boldsymbol{u}_x P_2\left(G_x, G_y, G_z\right) = 0.$$

Then the corresponding error equation equals

$$\mathbf{D}\boldsymbol{\varepsilon}_x = \mathbf{v}\boldsymbol{\beta}_x - \boldsymbol{u}_x \tag{7}$$

The term $\boldsymbol{\beta}_x = \left(\mathbf{A}^{\mathrm{T}}\mathbf{A}\right)^{-1}\mathbf{A}^{\mathrm{T}}u_x$ is derived using LS, where $\mathbf{A} = \left[\frac{\partial F_{u_x}}{\partial \boldsymbol{a}_i} \quad \frac{\partial F_{u_x}}{\partial \boldsymbol{b}_k}\right]$ (i = 0, 1, …, 19; k = 1, …, 19). We found that although the two methods are different in terms of the calculations, if $\mathbf{D}\mathbf{D}^{\mathrm{T}}$ is positive definite, the characteristics of matrix and structures of Equations (6) and (7) and their derivations are identical.

To benefit from the advantages of the two linearization methods, the hybrid linearized RFM can be derived as

$$\boldsymbol{u}_x = \mathbf{v}\boldsymbol{\beta}_x - \mathbf{D}\boldsymbol{\varepsilon}_x \tag{8}$$

Below, WTLS is used to obtain the coefficients in this hybrid model.

2.3. *Estimating RFM coefficients with iteration computation*

2.3.1. *WTLS estimation*

The WTLS estimator is used to estimate the RFM coefficients of the hybrid RFM. Compared to LS, the main advantage of WTLS is that it considers both errors of the observation vectors and errors of the coefficients. The derivation of WTLS estimation is

summarized as follows. In the EIV model, the observation equation is expressed as (Ge et al. 2006; Paige and Strakoš 2002; Schaffrin and Wieser 2008)

$$u = (\mathbf{v} - \mathbf{E_v})\boldsymbol{\beta} - \boldsymbol{\varepsilon_u} \tag{9}$$

where $u \in \mathrm{R}^{n\times 1}$ is the observation vector of dependent variable, $\boldsymbol{\varepsilon}_u \in \mathrm{R}^{n\times 1}$ is the observation error in dependent variable, $\boldsymbol{\beta} \in \mathrm{R}^{k\times 1}$ is the parameter vector, $\mathbf{v} \in \mathrm{R}^{n\times k}$ is the observation matrix based on independent variable ($n > k$), and $\mathbf{E_v} \in \mathrm{R}^{n\times k}$ is the random error matrix of $\mathbf{v}$.

Distributional characteristics of $\boldsymbol{\varepsilon}_u$ and $\mathbf{E_v}$ are equal to

$$\begin{bmatrix} \boldsymbol{\varepsilon}_u \\ \boldsymbol{\varepsilon}_\mathbf{v} = \mathrm{vec}(\mathbf{E_v}) \end{bmatrix} \sim \left(\begin{bmatrix} 0 \\ 0 \end{bmatrix}, \quad \sigma_0^2 \begin{bmatrix} \mathbf{Q}_u & 0 \\ 0 & \mathbf{Q_v} \end{bmatrix} \right) \tag{10}$$

where vec(.) is matrix straightening, σ_0^2 is the variance of the unit weight, and $\mathbf{Q_v}$ and $\mathbf{Q}_u$ are the variance–covariance matrices (inverse weight matrices) of $\boldsymbol{\varepsilon}_u$ and $\boldsymbol{\varepsilon_v}$, respectively. The relevant equations are

$$\mathbf{Q_v} = \mathbf{P}_0^{-1}, \quad \mathbf{Q}_u = \mathbf{Q}_0 \otimes \mathbf{Q_E} \tag{11}$$

in which $\mathbf{Q}_0 \in R^{k\times k}$, $\mathbf{Q_E} \in R^{n\times n}$ and $\otimes$ is the direct product of matrices. The result of the direct product is the variance–covariance matrix of errors in $\mathbf{v}$. This results in the objective function of WTLS as

$$\Phi_{\mathrm{WTLS}} = \boldsymbol{\varepsilon}_u{}^{\mathrm{T}}\mathbf{Q}_u^{-1}\boldsymbol{\varepsilon}_u + \boldsymbol{\varepsilon}_\mathbf{v}{}^{\mathrm{T}}\mathbf{Q}_\mathbf{v}^{-1}\boldsymbol{\varepsilon}_\mathbf{v} = \boldsymbol{\varepsilon}_u{}^{\mathrm{T}}\mathbf{P}_u\boldsymbol{\varepsilon}_u + \boldsymbol{\varepsilon}_\mathbf{v}{}^{\mathrm{T}}(\mathbf{Q}_0 \otimes \mathbf{Q_E})\boldsymbol{\varepsilon_v}. \tag{12}$$

To solve (12), we construct the following objective function based on Lagrange extreme conditions (Schaffrin and Wieser 2008; Schaffrin 2006),

$$\begin{aligned} \Phi(\boldsymbol{\varepsilon}_\mathrm{u}, \boldsymbol{\varepsilon_v}, \boldsymbol{\lambda}, \boldsymbol{\beta}) = {} & \boldsymbol{\varepsilon}_\mathrm{u}{}^{\mathrm{T}}\mathbf{P}_\mathrm{u}\boldsymbol{\varepsilon}_\mathrm{u} + \boldsymbol{\varepsilon}_\mathbf{v}{}^{\mathrm{T}}(\mathbf{Q}_0 \otimes \mathbf{Q_E})\boldsymbol{\varepsilon_v} \\ & + 2\boldsymbol{\lambda}^{\mathrm{T}}\left(u - \mathbf{v}\boldsymbol{\beta} - \boldsymbol{\varepsilon}_u + \left(\boldsymbol{\beta}^{\mathrm{T}} \otimes I_n\right)\boldsymbol{\varepsilon_v}\right) \end{aligned} \tag{13}$$

where $\boldsymbol{\lambda} \in R^{n\times 1}$ is the Lagrange operator and $\mathbf{E_v}\boldsymbol{\beta} = \left(\boldsymbol{\beta}^{\mathrm{T}} \otimes I_n\right)\boldsymbol{\varepsilon_v}$. Here, an iterative process is used to estimate the parameters of the Lagrange equations.

Step 1: Initial values definition.

$$\begin{cases} \boldsymbol{N} = \mathbf{v}^{\mathrm{T}}\boldsymbol{v}, \quad \boldsymbol{C} = \mathbf{v}^{\mathrm{T}}\boldsymbol{u} \\ \hat{\boldsymbol{\beta}}^{(0)} = \boldsymbol{N}^{-1}\boldsymbol{C} \\ \hat{\boldsymbol{\beta}}^{(1)} = \left(\mathbf{v}^{\mathrm{T}}\left(\mathbf{Q}_u + \left(\hat{\boldsymbol{\beta}}^{(0)}\right)^{\mathrm{T}}\mathbf{Q}_0\hat{\boldsymbol{\beta}}^{(0)}\mathbf{Q_E}{}^{-1}v\right)\mathbf{v}^{\mathrm{T}}(\mathbf{Q}_u + \left(\hat{\boldsymbol{\beta}}^{(0)}\right)^{\mathrm{T}}\mathbf{Q}_0\hat{\boldsymbol{\beta}}^{(0)}\mathbf{Q_E}\right)^{-1}u \end{cases} \tag{14}$$

Step 2: Iterative process.

$$\begin{cases} \boldsymbol{\theta}^{(i)} = \left(\mathbf{Q}_u + \left(\left(\hat{\boldsymbol{\beta}}^{(i)}\right)^{\mathrm{T}}\mathbf{Q}_0\hat{\boldsymbol{\beta}}^{(i)}\right)\mathbf{Q_E}\right)^{-1} \\ \hat{\boldsymbol{\lambda}}^{(i)} = \boldsymbol{\theta}^{(i)}\left(\boldsymbol{u} - \mathbf{v}\hat{\boldsymbol{\beta}}^{(i)}\right) \\ r^{(i)} = \left(\hat{\boldsymbol{\lambda}}^{(i)}\right)^{\mathrm{T}}\mathbf{Q_E}\hat{\boldsymbol{\lambda}}^{(i)} \\ \hat{\boldsymbol{\beta}}^{(i+1)} = \left(\mathbf{v}^{\mathrm{T}}\boldsymbol{\theta}^{(i)}\mathbf{v} - r^{(i)}\mathbf{Q}_0\right)^{-1}\mathbf{v}^{\mathrm{T}}\boldsymbol{\theta}^{(i)}\boldsymbol{u} \end{cases} \quad (i = 1, 2, 3, \ldots) \tag{15}$$

This process will repeat until $\hat{\boldsymbol{\beta}}^{(i)} - \hat{\boldsymbol{\beta}}^{(i-1)} < \tau$, where τ is a given threshold.

2.3.2. *WTLS-based RFM coefficients estimation and iterative computation*

WTLS takes into consideration the coordinate errors of image points and the errors of the coefficients. In the proposed model, they are derived from the errors of the observed coordinates of the image point $u = (u_x, u_y)$, and of the observed geodetic coordinates $g = (g_x, g_y, g_z)$.

In addition to the matrix error given by the GCP error of the coefficients $\mathbf{v}$, errors also appear in Equation (8) during its construction. Since errors in $\mathbf{D}$ are caused by $\boldsymbol{m}$, which is a part of $\mathbf{v}$, the errors in $\mathbf{D}$ will be reduced by minimizing errors in $\mathbf{v}$. To simplify the problem, the errors in $\mathbf{D}$ are ignored, and only the corresponding error matrix of $\mathbf{v}$ is considered.

Analogously, based on the parameters defined in Section 2.1, we have the following relationship:

$$\begin{cases} u_x = U_x - \boldsymbol{\varepsilon}_x \\ \boldsymbol{v} = \boldsymbol{V} - \boldsymbol{\varepsilon}_{\boldsymbol{v}} \end{cases} \tag{16}$$

Given n ($n \geq 39$) GCPs, the matrix form of the EIV regression model equals

$$\begin{cases} \boldsymbol{U}_x = V\boldsymbol{\beta}_x \\ \boldsymbol{U}_x = \boldsymbol{U}_x - \boldsymbol{\varepsilon}_x \\ \boldsymbol{v} = \boldsymbol{V} - \mathbf{E}_{\mathbf{v}} \end{cases} \tag{17}$$

Furthermore, by introducing the hybrid RFM linearization defined in Equation (8), the linear EIV model will be represented as

$$\boldsymbol{u}_x = (\mathbf{v} + \mathbf{E}_{\mathbf{v}})\boldsymbol{\beta}_x - \boldsymbol{\varepsilon}'_x = (\mathbf{v} + \mathbf{E}_{\mathbf{v}})\boldsymbol{\beta}_x - \mathbf{M}\mathbf{B}^{\mathrm{T}}\boldsymbol{\varepsilon}_x.$$

where $\mathbf{M} = [\boldsymbol{m}_1, \boldsymbol{m}_2, \ldots, \boldsymbol{m}_n]^{\mathrm{T}}$ and $\mathbf{B} = [\boldsymbol{b}_1, \boldsymbol{b}_2, \ldots, \boldsymbol{b}_n]^{T}$. The property of the errors is

$$\begin{bmatrix} \boldsymbol{\varepsilon}'_x \\ \boldsymbol{\varepsilon}_{\mathbf{v}} \end{bmatrix} \sim \left(\begin{bmatrix} 0 \\ 0 \end{bmatrix}, \begin{bmatrix} \mathbf{M}\mathbf{B}^{\mathrm{T}}\left(\mathbf{M}\mathbf{B}^{\mathrm{T}}\right)^{\mathrm{T}} \sum_{\boldsymbol{\varepsilon}_x} & 0 \\ 0 & \sum_{\mathbf{E}_{\mathbf{v}}} \end{bmatrix} \right) = \left(\begin{bmatrix} 0 \\ 0 \end{bmatrix}, \sigma_0^2 \begin{bmatrix} \mathbf{M}\mathbf{B}^{\mathrm{T}}\left(\mathbf{M}\mathbf{B}^{\mathrm{T}}\right)^{\mathrm{T}} \mathbf{P}_{\boldsymbol{\varepsilon}_x} & 0 \\ 0 & \mathbf{P}_{\mathbf{E}_{\mathbf{v}}} \end{bmatrix} \right)$$

We record $\sum_{\boldsymbol{\varepsilon}'_x} = \mathbf{M}\mathbf{B}^{\mathrm{T}}\left(\mathbf{M}\mathbf{B}^{\mathrm{T}}\right)^{\mathrm{T}} \sum_{\boldsymbol{\varepsilon}_x}$ and $\mathbf{P}_{\boldsymbol{\varepsilon}'_x} = \mathbf{M}\mathbf{B}^{\mathrm{T}}\left(\mathbf{M}\mathbf{B}^{\mathrm{T}}\right)^{\mathrm{T}} \mathbf{P}_{\boldsymbol{\varepsilon}_x}$, where $\mathbf{P}_{\boldsymbol{\varepsilon}_x} = \mathbf{P}_{0,\boldsymbol{\varepsilon}_x} \otimes \mathbf{P}_{\boldsymbol{\varepsilon}_x}$, $\mathbf{P}_{\mathbf{E}_{\mathbf{v}}} = \mathbf{P}_{0,\mathbf{E}_{\mathbf{v}}} \otimes \mathbf{P}_{\delta}$, and $\mathbf{P}_{0,\boldsymbol{\varepsilon}_x} \propto \mathrm{diag}\left(\sigma^2_{\boldsymbol{\varepsilon}_x}\right)$. To simplify the formulation of $\mathbf{P}_{0,\mathbf{E}_{\mathbf{v}}}$, we can set $(\boldsymbol{\Delta}_1, \boldsymbol{\Delta}_2, \boldsymbol{\Delta}_3, \boldsymbol{\Delta}_4) \triangleq (\delta_z, \delta_y, \delta_x, \varepsilon_x)$, where $\delta = (\delta_x, \delta_y, \delta_z)$ correspond to errors in ground coordinate and $\boldsymbol{\varepsilon} = (\boldsymbol{\varepsilon}_x, \boldsymbol{\varepsilon}_y)$ is the error in image coordinate. According to the variance covariance propagation law, the polynomial and structure of $\mathbf{V}$, it can be derived that

$$\mathbf{P}_{0,\mathbf{E}_{\mathbf{v}}} \propto \mathrm{diag}\left(\begin{bmatrix} \sum_1^4 \frac{\partial(\mathbf{E}_{\mathbf{v}}[1])}{\partial \boldsymbol{\Delta}_i} & \sum_1^4 \frac{\partial(\mathbf{E}_{\mathbf{v}}[2])}{\partial \boldsymbol{\Delta}_i} & \cdots & \sum_1^4 \frac{\partial(\mathbf{E}_{\mathbf{v}}[39])}{\partial \boldsymbol{\Delta}_i} \end{bmatrix} \right).$$

where $\mathbf{E}_{\mathbf{v}}[j]$ is the jth element of $\mathbf{E}_{\mathbf{v}}$, $j = 1, 2, \ldots, 39$. Thus, the objective function of WTLS-based RFM estimation turns into

$$\Phi_{\mathrm{WTLS}}\left(\hat{\boldsymbol{\beta}}_{x\,\mathrm{WTLS}}\right) = \boldsymbol{\varepsilon}'^{\mathrm{T}}_x \mathbf{W}_{\boldsymbol{\varepsilon}'_x} \boldsymbol{\varepsilon}'_x + \boldsymbol{\varepsilon}_{\mathbf{v}}{}^{\mathrm{T}} \mathbf{W}_{\mathbf{E}_{\mathbf{v}}} \boldsymbol{\varepsilon}_{\mathbf{v}} \tag{18}$$

where $\mathbf{W}_{\boldsymbol{\varepsilon}'_x} = \mathbf{W}_{0,\boldsymbol{\varepsilon}_x} \otimes \mathbf{W}_{\boldsymbol{\varepsilon}_x}\mathbf{W}_0$, $\mathbf{W}_{\mathbf{E}_\mathbf{v}} = \mathbf{W}_{0,\mathbf{E}_\mathbf{v}} \otimes \mathbf{W}_\delta$, $\mathbf{W}_{0,\boldsymbol{\varepsilon}_x} = \mathbf{P}_{0,\boldsymbol{\varepsilon}_x}^{-1}$, $\mathbf{W}_{0,\mathbf{E}_\mathbf{v}} = \mathbf{P}_{0,\mathbf{E}_\mathbf{v}}^{-1}$, $\mathbf{W}_0 = \left(\mathbf{M}\mathbf{B}^{\mathrm{T}}\left(\mathbf{M}\mathbf{B}^{\mathrm{T}}\right)^{\mathrm{T}}\right)^{-1}$ and,

$$\begin{cases} \mathbf{W}_{\boldsymbol{\varepsilon}_x} = \mathbf{P}_{\boldsymbol{\varepsilon}_x}^{-1} = \sigma_0^2 \sum_{\boldsymbol{\varepsilon}_x}^{-1} = \mathrm{diag}\left(w_{\varepsilon_{x_1}}, w_{\varepsilon_{x_2}}, \ldots, w_{\varepsilon_{xn}}\right), w_{\varepsilon_{x_i}} = \sigma_0^2 \Big/ \sigma_{\boldsymbol{\varepsilon}_{x_i}}^2 \\ \mathbf{W}_\delta = \mathbf{P}_\delta^{-1} = \sigma_0^2 \sum_\delta^{-1} = \mathrm{diag}(w_{\delta_1}, w_{\delta_2}, \ldots, w_{\delta_n}), w_{\delta_i} = \sigma_0^2 \Big/ \sigma_{\delta_i}^2 \end{cases} \quad i = 1, \ldots, n.$$

The solution $\hat{\boldsymbol{\beta}}_{x\,\mathrm{WTLS}}$ is the WTLS estimation of the EIV model in the x direction. Similarly, estimation in the y direction can also be derived, recorded as $\hat{\boldsymbol{\beta}}_{y\,\mathrm{WTLS}}$. Therefore, the WTLS estimator for hybrid RFM-based image orthorectification is determined as $\hat{\boldsymbol{\beta}}_{\mathrm{WTLS}} = \left(\hat{\boldsymbol{\beta}}_{x\,\mathrm{WTLS}}, \hat{\boldsymbol{\beta}}_{y\,\mathrm{WTLS}}\right)$. The WTLS estimator has no analytic closed-form solution in the general case; therefore, a numerical iterative optimization method can be employed to find the solution.

3. Experiments using a simulated data set

In this section, a simulation experiment is conducted with controlled settings to demonstrate the effectiveness of WTLS for RFM coefficients estimation. Estimation performance is assessed by comparing the results of simulation experiments using both LS and WTLS.

3.1. *Design of simulation experiment*

Four sections are included in this section: data preparation, adding errors and weight determination for GCPs, estimation and image correction, and precision evaluation. Orthorectification uses RFM to convert the reference image to the distortion image, and errors in the *x, y*, and *z* directions are simultaneously added to reference GCPs.

3.1.1. *Data preparation*

Elevation of the GCP is considered in the third-order RFM. Therefore, elevation values of pixels are randomly generated for the reference image to produce the corresponding elevation data. The simulated data in this experiment are with three dimensions but the generation of the distortion images is adapted from the idea of our previous works in Ge et al. (2012) and Wu et al. (2015). That is, the RFM coefficients $\boldsymbol{\beta}$ are known and used to transform the elevation data and the reference image, with a spatial resolution of 3 m and a size of 400 × 400 pixels, to obtain a corresponding system distortion image.

3.1.2. *Adding errors and weight determination for GCPs*

Error-free RCPs and TCPs (target GCPs) are generated from the reference image and distortion image, respectively. For validation, random errors are added to GCPs,

$$\begin{cases} g_x = G_x + \delta_x = G_x + \sigma_{\delta_x} \times r \times S_{xy} \\ g_y = G_y + \delta_y = G_y + \sigma_{\delta_y} \times r \times S_{xy} \\ g_z = G_z + \delta_z = G_x + \sigma_{\delta_z} \times r \times S_z \end{cases} \tag{19}$$

where $S_{xy} = 1\,\mathrm{m}$ and $S_z = 5\,\mathrm{m}$ denotes the resolutions in the *x, y* directions and *z* direction, respectively. *r* denotes a random number from a standard normal distribution $N(0,1)$. The errors of the RCPs in the *x, y*, and *z* directions follow the normal distributions

$N\left(0,\sigma_{\delta_x}^2\right)$, $N\left(0,\sigma_{\delta_y}^2\right)$, and $N\left(0,\sigma_{\delta_z}^2\right)$, respectively, and their standard deviations σ_{δ_x}, σ_{δ_y}, and σ_{δ_z} are determined by

$$\begin{cases} \sigma_{\delta_x} = \sigma_\delta \times \cos\left(\boldsymbol{\theta}_{1,\delta}\right) \times \cos\left(\boldsymbol{\theta}_{2,\delta}\right) \\ \sigma_{\delta_y} = \sigma_\delta \times \sin\left(\boldsymbol{\theta}_{1,\delta}\right) \times \cos\left(\boldsymbol{\theta}_{2,\delta}\right) \\ \sigma_{\delta_z} = \sigma_\delta \times \sin\left(\boldsymbol{\theta}_{2,\delta}\right) \end{cases} \tag{20}$$

where σ_δ, $\boldsymbol{\theta}_{1,\delta}$, and $\boldsymbol{\theta}_{2,\delta}$ follow the uniform distributions,

$$\begin{cases} \sigma_\delta \sim U\left[0,\sigma_{\delta,\max}\right] \\ \boldsymbol{\theta}_{1,\delta} \sim U[0,2\pi] \\ \boldsymbol{\theta}_{2,\delta} \sim U[0,2\pi] \end{cases} \tag{21}$$

According to the definition of the optimized weight for WTLS, the weights of the GCP containing errors $u = (u_x, u_y)$ and $g = (g_x, g_y, g_z)$ are

$$\begin{cases} \omega_{\boldsymbol{\varepsilon}} = \left[\sigma_0^2/\sigma_{\boldsymbol{\varepsilon}}^2\right]_{\text{normalized}} \\ \omega_\delta = \left[\sigma_0^2/\sigma_\delta^2\right]_{\text{normalized}} \end{cases} \tag{22}$$

where the variance scalar σ_0^2 is equal to 1.

3.1.3. *Image correction and precision evaluation*

The GCP data and their weights are centralized first; afterwards the input data are set to the corresponding correction model, followed by the estimation of the model coefficient $\hat{\boldsymbol{\beta}} = \left(\hat{\boldsymbol{\beta}}_x, \hat{\boldsymbol{\beta}}_y\right)$. Finally, a corrected image is obtained by using a correction technique.

Precision assessment is performed in two steps. (a) *Coefficient estimation*: the primary indices for evaluating precision and robustness are the variance of the estimated coefficient $\hat{\boldsymbol{\beta}}$, the bias, and the mean square error (MSE). (b) *Correction error*: the primary indices are the root mean squared error (RMSE) of the verification points (VPs) and the spatial variation (SV). For precision assessment, 32 VPs are chosen.

3.2. *Results of simulation experiment*

To validate the effectiveness of the proposed WTLS estimator, comparison has been conducted with LS and WLS. Monte Carlo simulation is used to express the uncertainties with a predefined input probability distribution. In this article, the Monte Carlo simulation was repeated 10,000 times on adding errors and weight determination.

3.2.1. *Analysing estimated coefficients*

Table 1 shows the mean values of the estimated coefficients. Figure 1 illustrates the variance, bias, and MSE in the different directions and calculated with LS, WLS, and WTLS for the Ortho-WTLS model. The variances in the *x* and *y* directions obtained with WTLS

Table 1. Summary of RMSE and SV of a 10,000-run Monte Carlo test.

Estimator	RMSE (m)	SV (m^2)
LS	1.3664 ± 0.3457	0.9675 ± 0.6722
WLS	1.1065 ± 0.2852	0.5841 ± 0.4106
WTLS	1.0397 ± 0.2838	0.5804 ± 0.4374

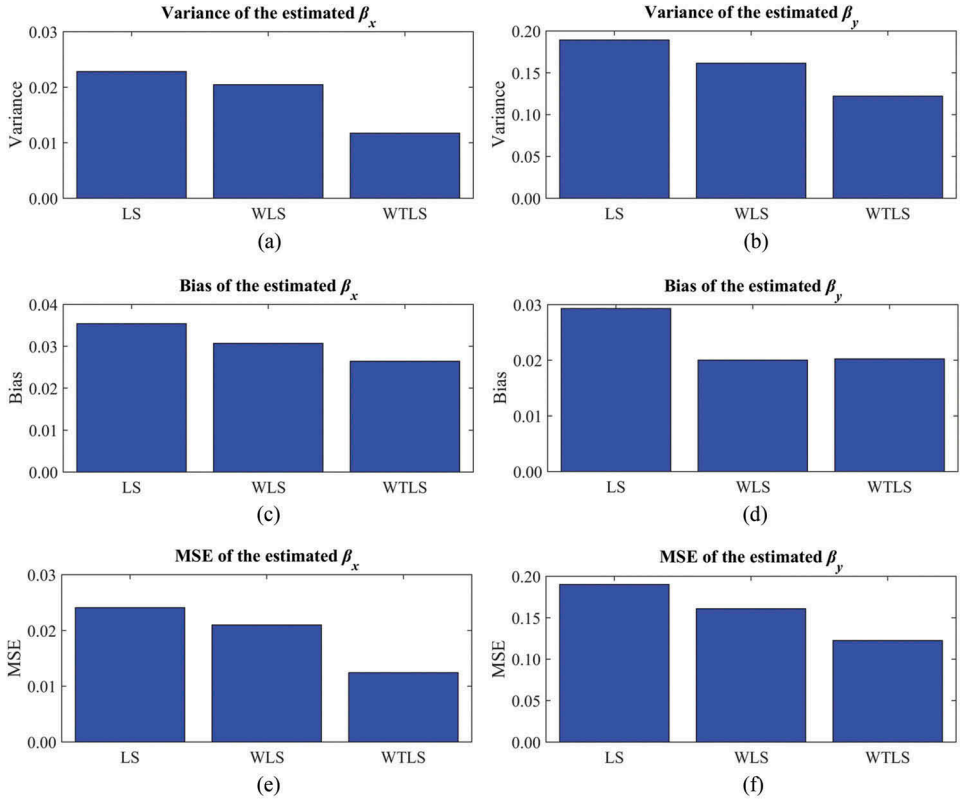

Figure 1. Comparison of estimated coefficients: variance, bias, and MSE values of the estimated β_x and β_y.

are equal to 0.0124 and 0.1216, and those calculated using LS are 0.0335 and 0.1894, WLS are 0.0201 and 0.1649, respectively. It demonstrates that WTLS is more robust when estimating coefficients as compared to LS and WLS. Biases and MSE in the two directions also show the superiority of the WTLS. Less bias is obtained by WTLS estimation because LS estimation is inconsistent and asymptotically biased if the RCP coordinates contain errors. In addition, the RMSE of WTLS is lower than that of LS and WLS, implying that WTLS is less affected by outliers. To conclude, WTLS provides a better coefficient estimation.

3.2.2. *Error analysis*

The precision indices, i.e. RMSE and SV, are discussed to further test the performance of image correction. Figures 2 and 3 show the RMSE and SV values for 200-run intervals of the 10,000-run Monte Carlo simulation experiment. The results are summarized in Table 1. As observed from Figure 2 and Table 1, the RMSEs calculated using WTLS are smaller than those calculated using LS and WLS, which reveals the superiority of WTLS in reducing correction errors. In addition, the errors produced by the WTLS estimator distribute more uniformly across the image, since the SV values of WTLS are smaller compared to LS and WLS, as can also be observed from Figure 3 and Table 1. When applied to the simulated

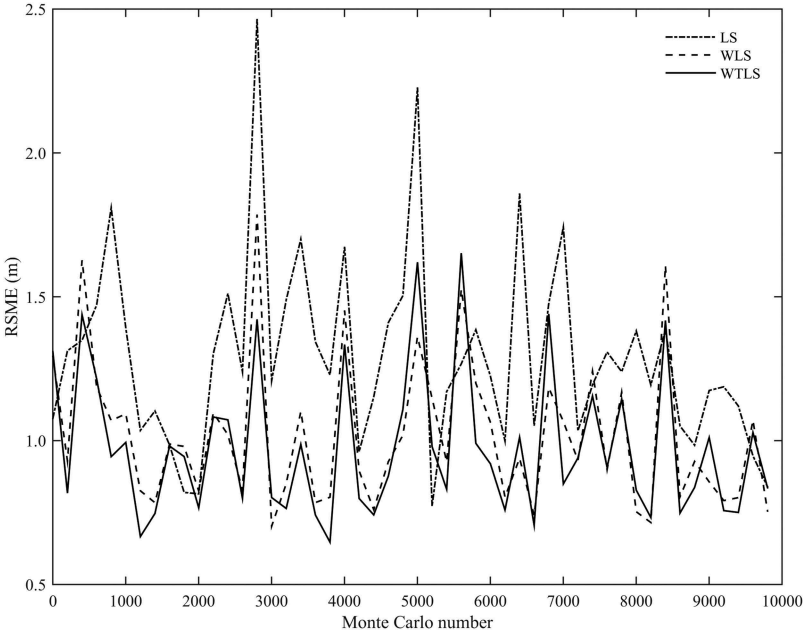

Figure 2. RMSE of a 10,000-run Monte Carlo test.

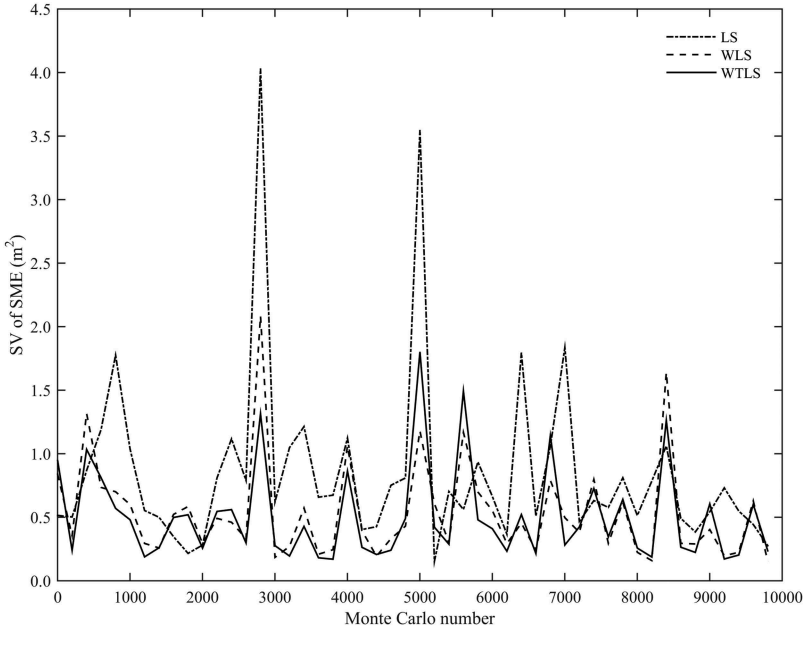

Figure 3. SV of SME of a 10,000-run Monte Carlo test.

image, WTLS provides a more robust parameter estimation for the RFM-based orthorectification and has a higher correction precision, compared with LS and WLS estimation, which cannot address the case wherein the RCP contain errors. In general, the Monte Carlo test shows that RSE and RMSE values of GCPs are large when they are located at the edges.

4. Experiments with a remote-sensing image

Compared with simulated images, distortions are more complex in remote-sensing images, leading to difficulties in recognizing and matching the corresponding points, especially if the spatial resolutions of the images are varied. Different from the manual collection in simulated experiment, the GCPs are commonly selected automatically (Abdelsayed, Ionescu, and Goodenough 1995; Likar and Pernuš 1999) using software such as ENVI. However, this may cause diverse precisions of errors of corresponding points and thus influence the correction precision. Therefore, we apply the proposed Ortho-WTLS method to real remote-sensing images to reduce the impact of heteroscedastic error contained in GCPs on orthorectification.

4.1. *Image data*

The test remote-sensing image was obtained from the Gaofen-1 satellite image covering the northwest region of Beijing (Changping County and Yanqing County) (Figure 4(a)). It was captured on 26 October 2013, with 16 m spatial resolution. The longitude and latitude of the top right corner of this image are 116°29′24.11″E and 40°41′31.07″N, and those of the lower left quarter of this image are 115°36′54.18″E and 40°1′21.52″N, respectively. The northeast and southwest regions are mountainous, and the southeast region is a plain. Due to the terrain fluctuations with elevation ranging from 20 to 2075 m, this region is fit for orthorectification experiment. To match the distortion image region, a corrected Landsat-8 image with a spatial resolution of 15 m obtained on 4 November 2013, is selected as the reference image (Figure 4(b)). The corresponding DEM is downloaded from an SRTM DEM and has a spatial resolution of 90 m (available here: http://www.gscloud.cn); these data were resampled to a consistent spatial resolution of 15 m for reference.

4.2. *Basic steps of image orthographic correction*

Step 1: Model selection. A third-order RFM is used for distortion image orthographic correction.

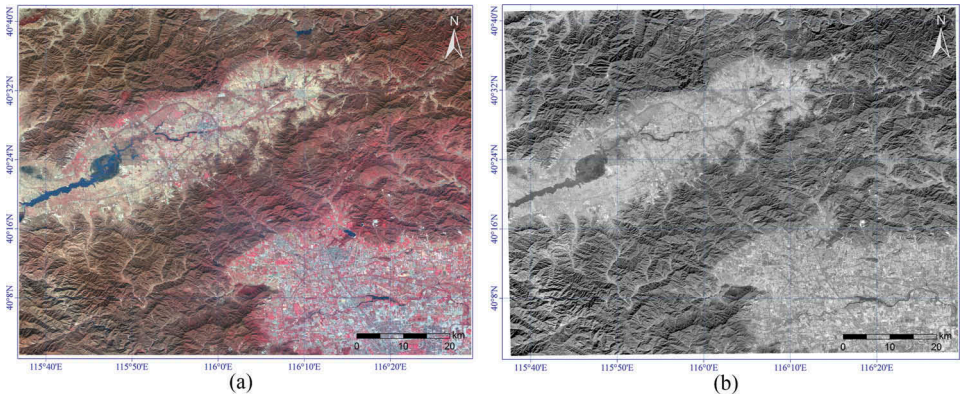

Figure 4. (a) Image I (the study area for correction: Gaofen-1 image) and (b) Image II (reference image: Landsat-8 image).

Step 2: GCP collection and weight determination. GCPs are automatically collected using automatic registration, by applying the image-to-image function in the MAP module of the ENVI4.8 software. Incorrectly matched GCPs and GCPs with large RMSEs (about 3 times the pixel's spatial resolution) are removed to reduce the errors. Different from simulation experiment, the weights of the GCPs are unknown in this image. Therefore, an adaptive optimization weight determination method is used to calculate the weights. First, an equal weight is set for each GCP during WTLS estimation initially. Then, the weight adjustment algorithm (Holland and Welsch 1977; Huber and Ronchetti 1981) is applied for estimating weights so that the weights of the GCPs can be revised. The primary idea is to estimate weights in the next step with the square error regression method after calculating the coordinate residuals of the RCP and TCP. However, due to the limitation of the RFM expression, the weights of the GCPs in the *z* direction, namely $\hat{u}_z$, cannot be estimated using the adaptive iteration method directly. This limitation lies in the relationship between the RCP $(g_x,\ g_y, g_z)$ and the TCP $(u_x,\ u_y)$ in the RFM that could only be estimated in *x* and *y* directions and can't be calculated in *z* direction. Therefore, to obtain the weights of the GCPs in the *z* direction, two procedures are adopted: (1) assuming no error occurs in GCPs in the *z* direction and only errors contained in the *x* and *y* direction; (2) using available GCPs of a higher accuracy in the *z* direction to assess the accuracy of GCPs in the *z* direction used in the RFM.

Step 3: Model estimation and image orthographic correction. Identical to the simulation experiment, LS, WLS, and WTLS are used to estimate the coefficients of the RFM. An orthographically corrected image is generated with the estimation method and resampling technique.

Step 4: Precision evaluation. The true values of the coefficients $\boldsymbol{\beta} = \left(\boldsymbol{\beta}_x, \boldsymbol{\beta}_y\right)$ and the true values of the reference VP coordinates are not available in real-world experiments. Therefore, statistical precision evaluation is used for correction. The true coordinate of the RCP $G = (G_x, G_y, G_z)$ is replaced by the observed coordinate $g = (g_x, g_y, g_z)$ to calculate the RMSE, in which the RSE of each VP is calculated as

$$\mathrm{RSE} = \sqrt{(\hat{g}_x - g_x)^2 + \left(\hat{g}_y - g_y\right)^2 + (\hat{g}_z - g_z)^2} \tag{23}$$

Because $\hat{g}_z$ is difficult to obtain as a result of the limitation of the RFM in this article, errors in the *z* direction are ignored, and Equation (23) can be written as

$$\mathrm{RSE} = \sqrt{(\hat{g}_x - g_x)^2 + \left(\hat{g}_y - g_y\right)^2} \tag{24}$$

4.3. *Experiments*

Three experiments are designed based on the above steps.

4.3.1. *Experiment 1*

To verify the orthorectification performance in flat area, the observations of the GCPs in the *z* direction are assumed to be without errors in this part. Thus, only the random errors in the *x* and *y* directions of the GCPs are considered.

According to *step 2*, data in this experiment are derived from the pre-processed GCPs automatically extracted by ENVI4.8. These data include 75 VPs with small residuals within 0.01 pixels, and 375 GCPs with a mean residual of 0.9 pixels, and a maximum residual of 1.2703 pixels. RMSE and SV values derived from the compared estimators with respect to increasing number of GCPs are plotted in Figures 5 and 6.

Figures 5 and 6 show that the increase in number of GCP pairs has a positive effect on registration precision to different extents. With an increasing number of GCPs, RMSE and SV values derived from the compared methods exhibit downward trends. We can also observe from Figure 2 that, compared with LS estimation, WTLS and WLS provide a more robust parameter estimation for the RFM-based orthorectification model. Benefit from the consideration of heteroscedastic data structures, WTLS outperforms WLS in terms of the correction precision. This superiority becomes more obvious when providing sufficient GCPs. A more detailed discussion on the impact of the number of GCPs, as well as the properties of LS and WTLS, is drawn in Part 5.

4.3.2. *Experiment 2*

In this part, data are considered to contain random errors in the *x, y*, and *z* directions as is the case in practice. The DEM with a spatial resolution of 25 m is regarded as the reference and is used to evaluate the errors of the SRTM DEM with a spatial resolution of 90 m. This relative error, together with the errors in *x* and *y* directions derived from the adaptive iteration method, is used to calculate the weight of each GCP and is introduced into the model calculation to verify the property of WTLS that the heteroscedastic data structures could be addressed.

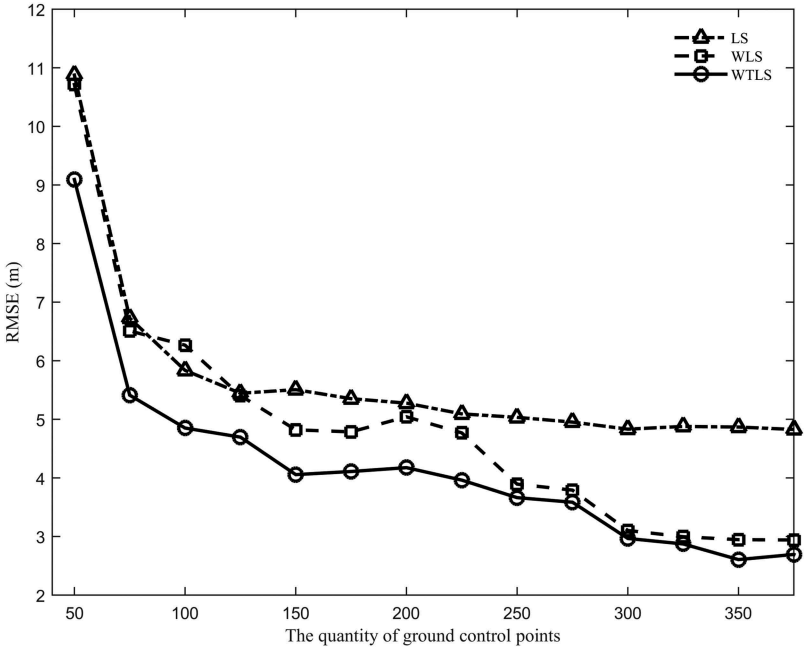

Figure 5. RMSE values derived from LS, WLS, and WTLS with increasing number of GCPs (without considering errors in the *z* direction).

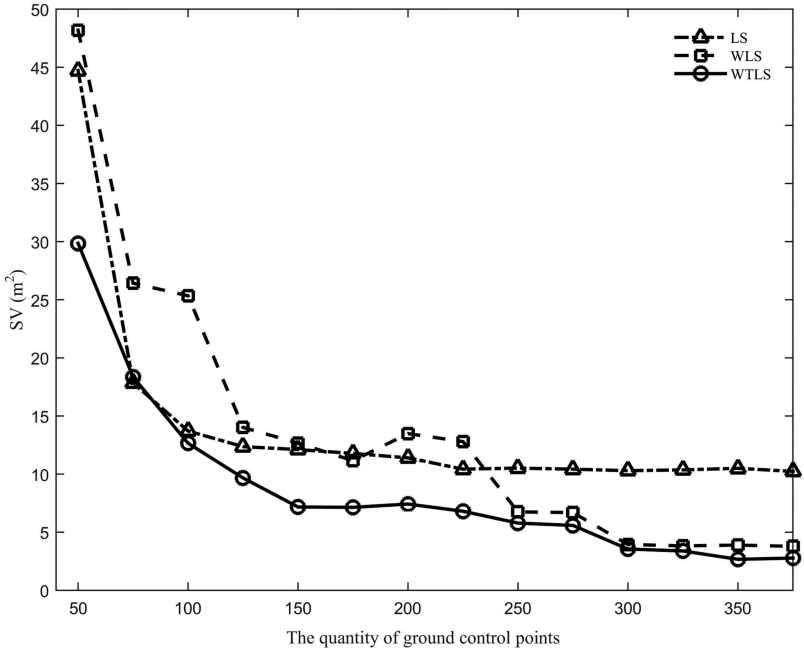

Figure 6. SV values derived from LS, WLS, and WTLS with increasing number of GCPs.

Figure 7(a) and Table 2 show that the RMSE value derived by WTLS (14.172 m) is larger than that by LS (11.031 m) if 50 GCP pairs are used; however, the RMSE values obtained by WTLS are all smaller than those obtained by LS if more than 75 GCP pairs are used. This result proves that WTLS performs inferior to LS if a small number of GCP pairs are used. As Figure 7(b) shows, although errors in the *z* direction have impact on WTLS method, leading to high RMSE values, those values are still lower than those obtained by LS if the numbers of GCPs are larger than 75. A primary reason to this phenomenon is that the quality of GCPs deteriorates for WTLS by adding errors in the *z* direction but LS is less affected, whereas due to robustness of WTLS in dealing with errors in GCPs, WTLS achieves better accuracy of errors in the *z* direction than LS when the number of GCPs increases. It should be noted that WLS slightly outperforms WTLS when the number of GCPs exceeds 175. Inferred from the error distribution map of GCPs in Figure 8, gross errors appear in the observation data (for instance, greater gross errors exist in *z* direction than *x*, *y* direction). The presence of gross error or errors with large variance has a negative effect on WTLS, resulting in a large deviation in the estimation from the true value. A further study on the weighting factor function will improve the robustness of WTLS for gross errors and errors with large variance.

The above results indicate that increasing the number of GCPs is beneficial for improving the orthorectification precision, if the levels of the GCP errors are similar, and the precision becomes stable if the number is sufficiently large (>375).

4.3.3. *Experiment 3*

Both quantity and quality of the GCPs on correction are considered in this experiment. A total of 400 GCPs with an average standard deviation of 1.4 pixels are recorded as GCP-

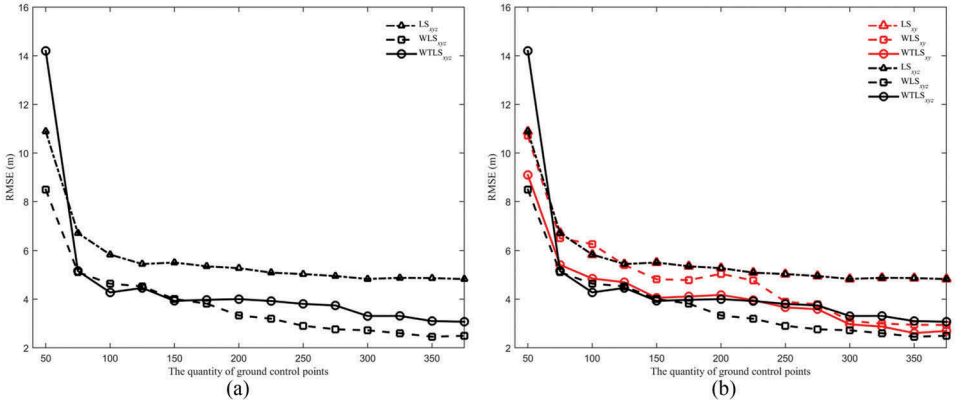

Figure 7. RMSE values derived from LS, WLS, and WTLS with increasing number of GCPs. (a) Results considering errors in the *z* direction. (b) Comparison on the results derived with and without considering errors in the *z* direction.

Table 2. RMSE and SV results of remote-sensing experiment 2.

Estimator	RMSE (m)	SV (m^2)
LS	4.8270	10.2400
WLS	2.9401	2.7116
WTLS	3.0719	4.3136

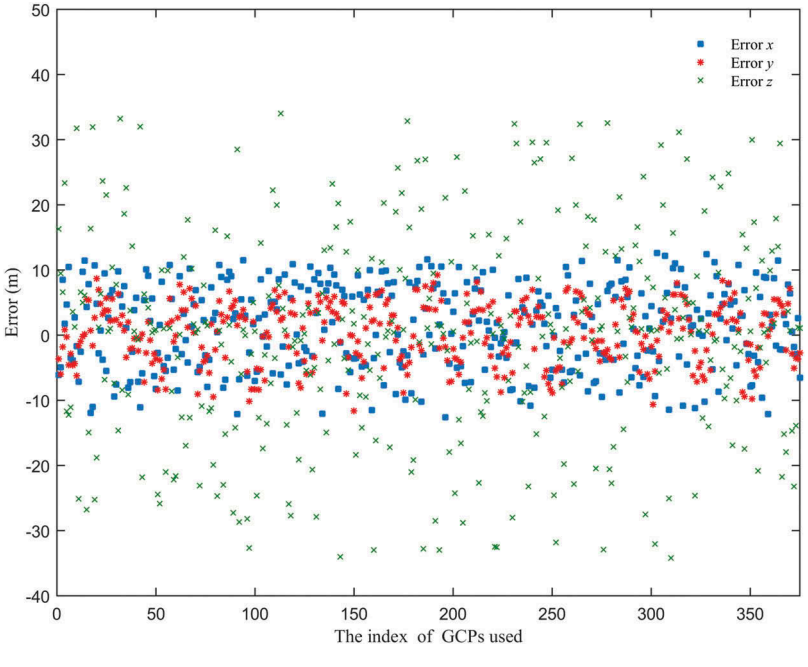

Figure 8. Distribution map of the errors in *x*, *y*, and *z* direction for GCPs used in experiment 2.

II-type data, where 125 GCP data sets with an average standard deviation of 0.9 pixels used in experiment 1 are recorded as GCP-I-type data. In this experiment, GCP-I-type

data are used initially, and RMSE values are calculated for LS, WLS, and WTLS with the number of GCPs increasing from 50 every 25 to 125. Then, the data sets of 25 uniformly distributed GCP-II-type are added to the 125 GCP-I-type data sets each time, and the corresponding RMSE values for the three estimators are calculated until the number of GCP-II-type data reaches 400. Finally, the effects of the quantity and quality of the GCPs on the orthorectification performance are analysed before and after gradually adding GCP-II-type data, and the performance of LS, WLS, and WTLS is evaluated.

Figure 9 illustrates that the correction result using LS with 125 GCPs of type-I data containing small errors can achieve a relatively low RMSE value of 5.4448 m; however, this value fluctuates after type-II data with large errors are gradually added. The RMSE value of LS first increases with the adding of GCP-II-type but decreases when the number of GCPs reaches 275. When the number of GCP-II-type data is sufficiently large, the RMSE value remains constant at 5.9 m. For the result generated by WLS and WTLS, the RMSE value decreases and becomes stable with the increase in GCP-II-type data. Compared to WLS, WTLS is more robust to the GCPs quality due to its consideration of heteroscedastic data structure. According to this result, the quality of the GCPs plays a more important role in image correction than its quantity for LS, whereas for WLS and WTLS, the effect of the quantity of GCPs is larger than that of the quality.

To conclude this section, the performance of LS, WLS, and WTLS are compared in the first experiment by only considering the random errors in the *x*- and *y*-direction. In order to establish a comparison close to the real-world condition, the second experiment considers the random errors in the z-direction in the simulation, and results shown in Table 2 confirm the superiority of the WTLS method. According to the first two

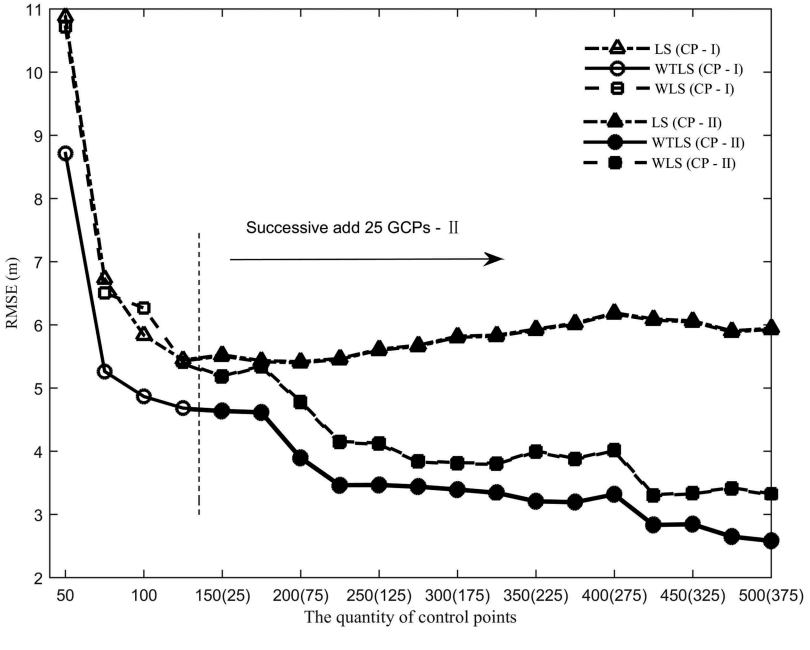

Figure 9. RMSE values of LS, WLS, and WTLS results when 25 GCPs of II type are gradually added to the 125 GCPs of I type (GCPs of I type: average standard deviation of approximately 0.9 pixels; GCPs of II type: average standard deviation of approximately 1.4 pixels).

experiments, the number of GCP pairs significantly influences orthorectification if the levels of the GCP errors are similar. In the last experiment, WTLS exhibits better accuracy than the compared methods with increasing number of GCPs of different precision levels, which briefly validate the robustness of the proposed WTLS.

4.4. *Discussion*

The above experiments show that WTLS can be reliably applied to orthorectification of real remote-sensing images, since it can effectively process errors with a heteroscedastic structure, with flexible weights strategy to balance the significances of RCPs and TCPs with various collecting precisions. Experimental results imply that the quantity and quality of GCPs play important roles in the orthorectification process. Detailed analyses on the impact of the GCPs' location errors and GCPs number have been discussed below.

4.4.1. *Impact of the errors on the GCPs' location*

In these experiments, the spatial resolution of the orthorectification image was 16 m, and that of a reference image was 15 m. During the GCP collection process, different spatial resolutions between the distortion image and the reference image resulted in difficulties when determining the precise locations of corresponding RCPs of TCPs. Thus, the location errors of the GCP pairs automatically collected with ENVI4.8 are inconsistent, even leading to incorrect image matching. Although we have removed the GCP pairs with large matching errors and assumed that the residual GCPs are properly matched, location errors were introduced and affected the estimation accuracy.

Assuming no errors in the z direction of the GCP data and that errors only occur in the x and y directions, it has been shown the superiority of image orthorectification with heteroscedastically structured errors within RCPs by comparing RMSE and SV values in Experiment 1. To further test the orthorectification of real GCP data, DEM data with high spatial resolution were used in Experiment 2 to depict errors in the z direction. Figure 10 and Table 2 show that if 50 GCP pairs are used, the SV value of the WTLS is larger than that of LS and WLS; however, it decreases if more than 75 pairs are used. For the 375-GCP-pair case, the SV value of WTLS (4.31 m) decreases by 57.91% as compared to LS (10.24 m). These results demonstrate that, when considering the error in the z direction, WTLS still performs better than LS in terms of RMSE and SV during image orthorectification if a large (>75) number of GCP pairs are used. These results indicate that WTLS is superior than LS in orthorectification if all types of GCP errors are considered.

The result obtained in Experiment 3 further shows that WTLS is preferable in addressing GCPs containing large errors and provides a more robust estimation than LS and WLS. According to Figure 10, the quality of the GCPs plays a more important role in image correction than its quantity for LS, whereas for WTLS, the effect of the quantity of GCPs is relatively larger than that of the quality.

4.4.2. *Impact of the numbers of GCPs on the orthorectification precision*

Experiment 1 shows that the RMSE and SV values derived from LS, WLS, and WTLS methods exhibit downward trends, with respect to the increase in GCPs numbers. According to Figure 5 and Figure 6, the rate of decrease is high if 50–150 GCPs are

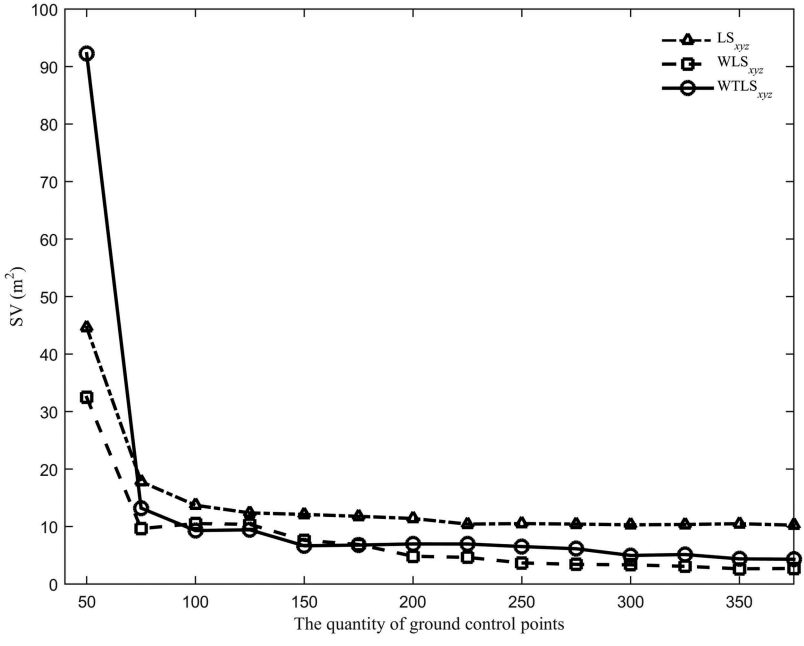

Figure 10. SV values derived from LS, WLS, and WTLS experiments with increasing number of GCPs.

used, whereas the rate is low for higher numbers. In particular, if more than 250 GCPs are used, the trend for the result is stable for LS. The figures suggest that WLS and WTLS perform better than LS, and their improvement will be enhanced if the number of GCPs is sufficiently large. This demonstrates the impact of the numbers of GCPs on the orthorectification precision. Next, WTLS is evaluated with 375 GCPs. In Table 3, the RMSE and SV values derived by WTLS are equal to 2.2926 m and 2.0790 m^2, representing decreases of 52.50% and 79.70% compared with those obtained by LS, i.e. 4.8270 m and 10.2400 m^2. Those derived by WLS are 2.9418 m and 3.7864 m^2. For LS, only the errors in the TCPs are considered; those in the RCPs are not, leading to inaccurate coefficient estimation. In addition, orthorectification of WTLS estimation is more precise.

According to Figure 7 obtained in experiment 2, if the number of GCPs increases, the advantage of WTLS on image orthorectification becomes more obvious by comparing the RMSEs containing estimation bias of DEM, i.e. Equation (23). In particular, if 375 pairs are used, the RMSE value derived by WTLS (3.0719 m, 44.30% are derived by the part of bias in the *z* direction) decreases by 36.36% compared to that derived by LS.

Moreover, GCPs with different precision levels were used in experiment 3 to further validate the effectiveness of the proposed method. The comparison demonstrates that orthorectification precision can be improved and becomes stable with an increasing

Table 3. RMSE and SV results of remote-sensing experiment 1.

Estimator	RMSE (m)	SV (m^2)
LS	4.8270	10.2400
WLS	2.9418	3.7864
WTLS	2.2926	2.0790

number of GCPs if the observation precisions of the GCPs are identical. If low-precision GCPs are added to a high-precision GCP data, orthorectification precision may not improve. In addition, WTLS is robust for processing such GCPs with highly different error precisions; however, LS is sensitive to such data.

It is common in practice that large amount of GCP pairs can be collected automatically or manually but are in different precision levels. According to the above experiment results, the proposed WTLS technique is robust to the quantity and quality of GCPs and, thus, potential to provide more precise orthorectification results.

5. Conclusion

In this article, a new RFM based on WTLS estimation is presented for orthorectification of remotely sensed image, aiming at addressing the case that RCPs and TCPs have heteroscedastically structured errors. This commonly happens if the coordinates of the RCPs and TCPs contain errors of an unequal accuracy, e.g. when they are acquired manually or automatically. The proposed Ortho-WTLS method is designed to address the challenge of a biased sample. This study showed that it can obtain more precise and robust orthorectification results than using commonly used LS and WLS in terms of variance, bias, and MSE values. In particular, the experiment considering real remote-sensing images found that orthorectification results obtained from adaptive weight determination and WTLS-based RFM estimation is more reliable than LS-based RFM estimation, which is validated by comparisons of RMSE and SV values. This article further tested the impact of the quantity and quality of GCPs in image orthorectification. Results show that both quantity and quality of GCPs played a key role in obtaining accurate estimation results. Orthorectification precision increased with an increasing number of GCPs of identical precision levels but remained stable after reaching a maximum value. For GCPs of different precision levels, Ortho-WTLS could generate more stable and precise results. In conclusion, Ortho-WTLS is an effective and reliable image orthorectification method for the RCPs and TCPs containing heteroscedastically structured errors in the coordinates.

The results obtained from the simulated and real remote-sensing images are encouraging. It remains challenging to improve the efficiency of weight determination for GCPs. A potential solution lies in the evaluation of the spatial weights of GCPs from local neighbours by considering their spatial autocorrelations. This needs further study and could be done by sample partitioning and adapt the evaluation procedures.

Acknowledgements

This research was supported in part bythe National Key Technology Research and Development Program of the Ministry of Science and Technology of China: [Grant Number 2012BAH33B01], and in part by the Knowledge Innovation Program of the Chinese Academy of Sciences: [Grant Number KZCX2-EW-QN303], and the National Natural Science Foundation of China: [Grant Numbers 41471296, 41601389]. The authors are grateful to two anonymous referees for their constructive comments, which helped to improve the quality of the article.

Disclosure statement

No potential conflict of interest was reported by the authors.

Funding

This research was supported in part by the National Key Technology Research and Development Program of the Ministry of Science and Technology of China: [Grant Number 2012BAH33B01], and in part by the Knowledge Innovation Program of the Chinese Academy of Sciences: [Grant Number KZCX2-EW-QN303], and the National Natural Science Foundation of China: [Grant Numbers 41471296, 41601389].

References

Abdelsayed, S., D. Ionescu, and D. Goodenough. 1995. "Matching and Registration Method for Remote Sensing Images." Paper presented at the Geoscience and Remote Sensing Symposium, 1995. IGARSS'95.'Quantitative Remote Sensing for Science and Applications', International, Firenze, Italy, July 10–14.

Consortium, OpenGIS. 1999. *The OpenGIS® Abstract Specification Topic 6: The Coverage Type and Its Subtypes Version 4*. Wayland, MA, USA: OpenGIS Consortium.

Consortium, OpenGIS. 2004. *The OpenGIS® Abstract Specification. Topic 7: Earth Imagery*. Wayland, MA, USA: OpenGIS Consortium.

Dave, C. P., R. Joshi, and S. S. Srivastava. 2015. "A Survey on Geometric Correction of Satellite Imagery." *International Journal of Computer Applications* 116: 24–27. doi:10.5120/20389-2655.

Dowman, I., and J. T. Dolloff. 2000. "An Evaluation of Rational Functions for Photogrammetric Restitution." *International Archives Photogramm Remote Sensing* 33 ((B3/1; PART 3)): 254–266.

Ge, Y., T. J. Wu, J. H. Wang, J. H. Ma, and Y. Y. Du. 2012. "Scaled Total-Least-Squares-Based Registration for Optical Remote Sensing Imagery." *Earth Sciences Informatics* 5 (3–4): 137–152. doi:10.1007/s12145-012-0103-1.

Ge, Y., Y. Leung, M. Jianghong, and J. Wang. 2006. "Modelling for Registration of Remotely Sensed Imagery When Reference Control Points Contain Error." *Science in China Series D* 49 (7): 739–746. doi:10.1007/s11430-006-0739-0.

Gong, D. C., and Y. S. Zhang. 2003. "The Solving and Application of Rational Function Model." *Journal of the Surveying and Mapping Division: Proceedings of the American Society of Civil Engineers* 20 (1): 39–42.

Holland, P. W., and R. E. Welsch. 1977. "Robust Regression Using Iteratively Reweighted Least-Squares." *Communicable Statistical* 6 (9): 813–827. doi:10.1080/03610927708827533.

Huber, P. J., and E. M. Ronchetti. 1981. *Robust Statistics, Ser*. New York, NY: Wiley.

Li, S., S. Dragicevic, F. A. Castro, M. Sester, S. Winter, A. Coltekin, C. Pettit, B. Jiang, J. Haworth, and A. Stein. 2016. "Geospatial Big Data Handling Theory and Methods: A Review and Research Challenges." *ISPRS Journal of Photogrammetry and Remote Sensing* 115: 119–133. doi:10.1016/j.isprsjprs.2015.10.012.

Likar, B., and P. Franjo. 1999. "Automatic Extraction of Corresponding Points for the Registration of Medical Images." *Medical Physics* 26 (8): 1678–1686. doi:10.1118/1.598660.

Markovsky, I., M. L. Rastello, A. Premoli, A. Kukush, and V. H. Sabine. 2006. "The Element-Wise Weighted Total Least-Squares Problem." *Computational Statistics & Data Analysis* 50 (1): 181–209. doi:10.1016/j.csda.2004.07.014.

Matei, B. C., and P. Meer. 2006. "Estimation of Nonlinear Errors-In-Variables Models for Computer Vision Applications." *Ieee Transactions on Pattern Analysis and Machine Intelligence* 28 (10): 1537–1552. doi:10.1109/TPAMI.2006.205.

Paige, C. C., and S. Zdenek. 2002. "Scaled Total Least Squares Fundamentals." *Numerische Mathematik* 91 (1): 117–146. doi:10.1007/s002110100314.

Qin, X. W., S. F. Tian, Y. T. Hong, and G. Zhang. 2005. ""The Algorithm for Parameters of RPC Model without Initial Value "." *Remote Sensing Land Resources* 66 (4): 7–10.

Richards, J. A., and X. P. Jia. 1999. *Remote Sensing Digital Image Analysis: An Introduction*. 3rd ed. New York, NY: Springer.

Schaffrin, B. 2006. "A Note on Constrained Total Least-Squares Estimation." *Linear Algebra and Its Applications* 417 (1): 245–258. doi:10.1016/laa.2006.03.044.

Schaffrin, B., and A. Wieser. 2008. "On Weighted Total Least-Squares Adjustment for Linear Regression." *Journal Geod* 82 (7): 415–421. doi:10.1007/s00190-007-0190-9.

Tao, C. V., and Y. Hu. 2001a. "A Comprehensive Study of the Rational Function Model for Photogrammetric Processing." *Photogramm Engineering Remote Sensing* 67 (12): 1347–1357.

Tao, C. V., and Y. Hu. 2001b. 3-D Reconstruction Algorithms with the Rational Function Model and Their Applications for Ikonos Stereo Imagery. Paper presented at the Proceedings of Joint ISPRS Workshop on High Resolution Mapping from Space, Hannover, Germany, September 19–21.

Tong, X., Y. Jin, and L. Lingyun. 2011. "An Improved Weighted Total Least Squares Method with Applications in Linear Fitting and Coordinate Transformation." *Journal of Surveying Engineering* 137 (4): 120–128. doi:10.1061/(ASCE)SU.1943-5428.0000055.

Toutin, T. 2003. "Geometric Correction of Remotely Sensed Images." In *Remote Sensing of Forest Environments: Concepts and Case Studies*, edited by M. Wulder and S. E. Franklin, 143–180. Norwell, MA: Kluwer Academic Publishers.

Toutin, T. 2004. "Review Article: Geometric Processing of Remote Sensing Images: Models, Algorithms and Methods." *International Journal of Remote Sensing* 25 (10): 1893–1924. doi:10.1080/0143116031000101611.

Van Huffel, S., and J. Vandewalle. 1991. *The Total Least Squares Problem: Computational Aspects and Analysis*. Vol. 9. Philadelphia, PA: Siam.

Wansbeek, T., and E. Meijer. 2000. *Measurement Error and Latent Variables in Econometrics*. Amsterdam: Elsevier.

Wu, T. J., Y. Ge, J. H. Wang, A. Stein, Y. Z. Song, Y. Y. Du, and J. H. Ma. 2015. "A WTLS-Based Method for Remote Sensing Imagery Registration." *IEEE Transactions Geoscience Remote Sensing* 53 (1): 102–116. doi:10.1109/TGRS.2014.2318705.

Yang, X. 2000. Accuracy of Rational Function Approximation in Photogrammetry. Paper presented at the ASPRS annual conference, Washington DC, May 22–26.